Journal of Luminescence 188 (2017) 541–550

Contents lists available at ScienceDirect

Journal of Luminescence

journal homepage: www.elsevier.com/locate/jlumin

Optical spectroscopy and modeling of Fe^{2+} ions in zinc selenide

Jonathan W. Evans[a,*], Thomas R. Harris[a], B. Rami Reddy[b], Kenneth L. Schepler[c], Patrick A. Berry[a]

[a] Air Force Research Laboratory, Sensors Directorate, WPAFB OH 45433, United States
[b] Alabama A & M University, Normal, AL 35762, United States
[c] CREOL, University of Central Florida, Orlando, FL 32816, United States

ARTICLE INFO

JEL:
37N20
78A60

Keywords:
Laser Spectroscopy
Transition Metals
Modeling
Mid-IR laser materials

ABSTRACT

In this work, we collect absorption and emission spectra for Fe^{2+} ions in zinc selenide (Fe:ZnSe) and identify trends from 10.5 to 300 K in absorption and from 5 to 300 K in emission. The absorption spectrum is used to determine free parameters in historical eigenvalue expansions for Fe^{2+} ions in tetrahedral potentials as described by Slack, Ham, and Chrenko. Additionally, we measure the change of the fluorescence lifetime of Fe^{2+} ions in ZnSe with respect to temperature from 5 to 300 K. A model of the behavior is developed and fit to the collected lifetime data. Results are compared with previously published values of the fluorescence lifetime of Fe:ZnSe and notable discrepancies are attributed to concentration-dependent effects.

1. Background

Fe:ZnSe lasers have been demonstrated in various regimes, including gain-switched [1,2], continuous-wave [3,4], and Q-switched operation [5]. Furthermore, laser output from Fe:ZnSe has been demonstrated to be broadly tunable across its fluorescence band of 3800–5000 nm [6–8]. Because of this flexibility, Fe:ZnSe is rapidly becoming an important mid-IR laser gain medium for medical, scientific, and military applications. This flexibility stems from the optical behavior of tetrahedrally coordinated Fe^{2+} ions as originally explained by Low and Weger [9].

Slack, Ham, and Chrenko (SHC) [10] later extended the model of Low and Weger to include a dynamic Jahn–Teller effect and used it to explain the low temperature absorption spectra of Fe:ZnS and Fe:CdTe. In addition, SHC offered an 'alternative' assignment of the observed Fe:ZnS absorption spectrum which they considered to be unlikely at the time, but which Ham and Slack later accepted [11]. In this work, we use this model to explain the structure of a high-resolution absorption spectrum of Fe:ZnSe at 10.5 K. We create an approximation to the observed spectrum by careful consideration of transition strengths, thermal statistics, and the phonon density of states in ZnSe as calculated from inelastic neutron scattering (INS) data [12–14].

Slack and O'Meara [15], and later Ham and Slack [11], applied this model to the low temperature emission spectrum of Fe:ZnS. In this work, we use this model to explain the structure of a high-resolution emission spectrum of Fe:ZnSe at 5 K. We show that our assignment of the absorption spectrum of Fe:ZnSe is consistent with the observed emission spectrum. In addition to the low temperature spectra, we present high-resolution absorption and emission spectra of Fe:ZnSe, from 10 to 300 K and 5–225 K respectively.

Several authors have investigated the temperature dependence of the fluorescence lifetime of Fe^{2+} ions in ZnSe grown from melt [1,16,17] and observed a maximum lifetime of approximately 105 μs near 120 K. However, Myoung et al. have observed the maximum lifetime of Fe^{2+} ions doped by diffusion into CVD-grown polycrystalline ZnSe to be approximately 60 μs at 100 K. To date, the large difference between these observations has not been explained, though it has been hypothesized that the difference is due to fact that Myoung's material was doped by post-growth diffusion rather than grown from melt. In this work, we further investigate the optical behavior of Fe:ZnSe samples prepared by diffusion, including measurement of the fluorescence lifetime of the Fe^{2+} ions. We confirm the result of Myoung et al. and we develop a model that explains the differences observed between Fe:ZnSe crystals, which we attribute to dopant concentration.

2. Theory

Iron atoms substitute for the group II atom when they are doped into the matrix of II–VI crystals such as ZnSe. They take on the 2+ ionization state and their electronic configuration becomes d^6. This configuration gives rise to term symbols which are, in descending order of energy (by Hund's rules), ^1D,^1F,^1G,^1I,^1S,^3D,^3F,^3G,^3H,^3P, and ^5D [18]. Group theory predicts that the 25-fold degenerate ^5D ground level is split by the tetrahedral crystal field of its cubic host to form a 15-fold

* Corresponding author.
E-mail address: jonathan.evans.6@us.af.mil (J.W. Evans).

http://dx.doi.org/10.1016/j.jlumin.2017.04.017
Received 11 October 2016; Received in revised form 27 February 2017; Accepted 4 April 2017
Available online 17 April 2017

degenerate $^5T_2$ level and a 10-fold degenerate ^5E level [9]. For Fe^{2+} ions, the $^5T_2$ level is greater in energy than the ^5E level by the crystal field energy $10Dq \approx 3000\,cm^{-1}$ [19], which is much less than the bandgap energy of ZnSe ($>2 \times 10^4\,cm^{-1}$).

Low and Weger [9] have shown that the $^5T_2$ level is equivalent to a ^3D level and splits into three sublevels with $J' = 3$, $J' = 2$, and $J' = 1$ (these are labeled Γ_1, Γ_2, and Γ_3 respectively in Bethe's notation [20]) under the influence of the first-order spin–orbit interaction. Those levels are further split by the second-order interaction. The Γ_1 level splits into three sublevels: Γ_1, Γ_4, and Γ_5. The Γ_2 level splits into two sublevels: Γ_3 and Γ_4. The Γ_3 level is transformed into another single sublevel Γ_5. The sublevels Γ_1, Γ_4, Γ_5, Γ_3, Γ_4 and Γ_5 have degeneracies 1, 3, 3, 2, 3, and 3 respectively. Low and Weger have shown that the ^5E level is not split by the first-order interaction, but is split by the second order interaction into five sublevels Γ_2, Γ_5, Γ_3, Γ_4, and Γ_1 with degeneracies 1, 3, 2, 3, and 1 respectively. From this point forward, we have adopted the primed notation for repeated $^5T_2$ levels and the lowercase notation for labeling the ^5E levels introduced by Rivera-Iratchet et al. [21] to avoid ambiguity in the labeling of levels and transitions.

Udo et al. extended the theory of Low and Weger by performing perturbation theory calculations for the spin–orbit coupling out to the fourth order [22]. They give the eigenvalues of the Γ_m sublevels of $^5T_2$ as

$$
\begin{aligned}
E_{\Gamma_1} &= \Delta - 2\lambda + 24\frac{\lambda^2}{\Delta}(1-2\sigma - 20\sigma^2)\\
E_{\Gamma'_4} &= \Delta - 2\lambda + 12\frac{\lambda^2}{\Delta}(1-20\sigma^2)\\
E_{\Gamma'_5} &= \Delta - 2\lambda + \frac{12}{5}\frac{\lambda^2}{\Delta}\left(1-\frac{32}{25}\sigma - \frac{4442}{625}\sigma^2\right)\\
E_{\Gamma_3} &= \Delta + \lambda + 12\frac{\lambda^2}{\Delta}\left(1 + \sigma - 11\sigma^2\right)\\
E_{\Gamma_4} &= \Delta + \lambda + 6\frac{\lambda^2}{\Delta}\left(1-3\sigma - 5\sigma^2\right)\\
E_{\Gamma_5} &= \Delta + 3\lambda + \frac{18}{5}\frac{\lambda^2}{\Delta}\left(1 + \frac{63}{25}\sigma + \frac{4003}{625}\sigma^2\right),
\end{aligned}
\tag{1}
$$

and the γ_n sublevels of ^5E as

$$
\begin{aligned}
E_{\gamma_2} &= 0\\
E_{\gamma_5} &= -6\frac{\lambda^2}{\Delta}\left(1 + \sigma + \sigma^2\right)\\
E_{\gamma_3} &= -12\frac{\lambda^2}{\Delta}\left(1 + \sigma - 11\sigma^2\right)\\
E_{\gamma_4} &= -18\frac{\lambda^2}{\Delta}\left(1-\sigma - 15\sigma^2\right)\\
E_{\gamma_1} &= -24\frac{\lambda^2}{\Delta}\left(1-2\sigma - 20\sigma^2\right)
\end{aligned}
\tag{2}
$$

with $\Delta = 10Dq$ and λ as parameters and with $\sigma = |\lambda|/\Delta$.[1] From the expressions for the eigenvalues of the system we can generate the energy level diagram as seen in Fig. 1.

Both Udo et al. and SHC performed calculations of the electric dipole moment of each $\gamma_n \leftrightarrow \Gamma_m$ transition using approximate wavefunctions for the Fe^{2+} ion in a tetrahedral potential. From this calculation, they generate the selection rules for these transitions as well as their relative transition dipole moments. The allowed transitions are shown in Fig. 2. From this calculation, we expect nineteen distinct transition lines to be observed in the absorption and emission spectra of Fe:ZnSe

[1] Note that an equivalent expansion was performed by SHC [10], who used different parameters ζ, μ, and ρ which are related to Δ and λ by the relations $\zeta = -\lambda + 2\lambda^2/\Delta$, $\mu = 2\lambda^2/\Delta$, and $\rho = -6\lambda^2/\Delta$.

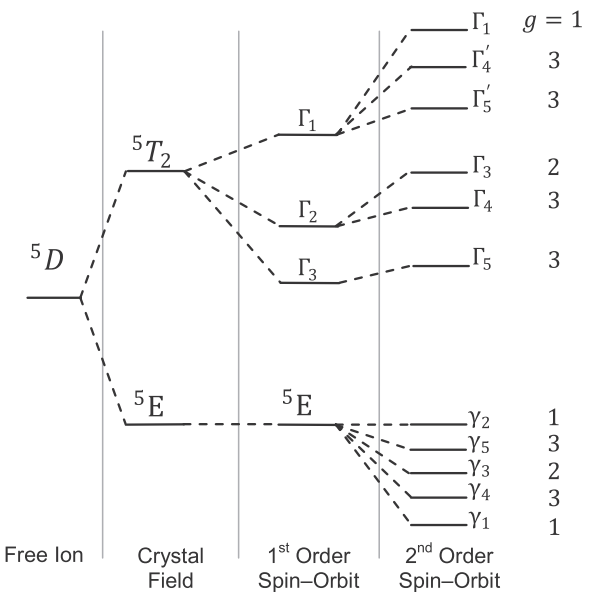

Fig. 1. The energy level diagram of an Fe^{2+} ion in a tetrahedral field with spin–orbit coupling. g is the degeneracy of the level.

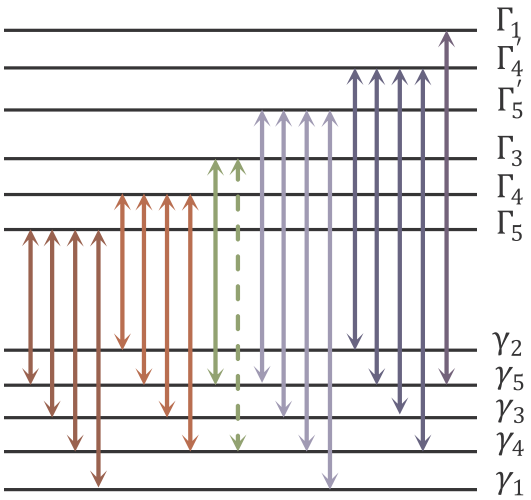

Fig. 2. Allowed transitions between spin–orbit split levels of the Fe^{2+} ion in a tetrahedral crystal field. The $\gamma_4 \leftrightarrow \Gamma_3$ transition is shown as a dashed line because its oscillator strength is zero according to Udo [22].

at low temperatures. However, as will be shown later, the eigenenergies and dipole moments calculated for the spin–orbit model fail to account for the structure of the observed absorption spectrum of Fe:ZnS (see [10]) and Fe:ZnSe.

SHC have shown that the aforementioned failure of the spin–orbit model to describe the observed absorption spectrum of Fe:ZnS can be explained by the dynamic Jahn–Teller (DJT) effect [10]. This effect has been simulated by other researchers [11,23,24], and plays a significant role in determining the structure observed in the absorption spectrum of Fe:ZnSe. The DJT effect dramatically increases the coupling of the electronic Hamiltonian of the Fe^{2+} ion to the vibrational Hamiltonian of the crystal host. The result of this coupling is *spin–orbit quenching*, which is characterized by a reduction in the energy separation between the Γ_m levels. In addition to this increased electron–phonon coupling, the DJT effect induces a substantial modification of the dipole moments of the electronic transitions.

Quantitatively, these effects can be observed in several ways. First, spin–orbit interactions are quenched such that $\zeta \rightarrow \zeta' = \zeta Q$ and

Table 1
The relative dipole moment of each $\gamma_n \leftrightarrow \Gamma_m$ transition, including the DJT correction of SHC [10]. The values have been calculated averaging over the degeneracies in γ levels and adding over them for Γ levels. We have introduced β to describe the salient reduction of Van Vleck [25], which affects transitions to and from $J' \neq 1$ states.

Final Level Initial Level	Γ_1	Γ'_4	Γ''_5
γ_2	–	$\frac{\beta}{2}(1-y)$	–
γ_5	$\frac{2\beta}{9}$	$\frac{\beta}{12}(1+y)$	$\frac{\beta}{12}(1-x)$
γ_3	–	$\frac{\beta}{4}(1-y)$	$\frac{\beta}{4}(1+x)$
γ_4	–	$\frac{\beta}{4}(1+y)$	$\frac{\beta}{4}(1-x)$
γ_1	–	–	$\frac{\beta}{2}(1+x)$
Final Level Initial Level	Γ_3	Γ_4	Γ_5
γ_2	–	$\frac{\beta}{2}(1+y)$	–
γ_5	$\frac{4\beta}{9}$	$\frac{\beta}{12}(1-y)$	$\frac{1}{12}(1+x)$
γ_3	–	$\frac{\beta}{4}(1+y)$	$\frac{1}{4}(1-x)$
γ_4	–	$\frac{\beta}{4}(1-y)$	$\frac{1}{4}(1+x)$
γ_1	–	–	$\frac{1}{2}(1-x)$

$\rho \rightarrow \rho' = \rho(1+W)/2$ (see Footnote 1), where $0 \leq Q \leq 1$ and $0 \leq W \leq 1$ (see [10]). Second, the transition dipole moments are drastically lowered and modified by parameters x and y as given in Table 1 (see [10]). Van Vleck has noted that the drastic lowering of the transition dipole moment is itself quenched by the spin–orbit interaction for transitions to and from $J' = 1$ states (e.g. Γ_5) [25]. Third, the DJT effect dramatically increases the coupling of the electronic Hamiltonian of the Fe^{2+} ion to the vibration of the crystal host. Thus each of the Γ and γ sublevels becomes the ground state of a multidimensional harmonic oscillator whose 'rungs' are integer multiples of the phonon energies of the crystal host. Thus the DJT coupling leads to the creation of many *vibronic* levels in the $^5T_2$ and ^5E manifolds, which are evident in the absorption and emission spectra respectively (see Sections 3 and 4).

3. Absorption spectroscopy

A Nicolet 6700 series Fourier transform infrared spectrometer (FTIR) was used to collect the absorption spectrum of a sample of Fe:ZnSe with a thickness of 1.6 mm. This CVD-grown ZnSe sample was diffusion-doped with Fe^{2+} ions to a concentration of approximately 4.6×10^{18} cm^{-3} by IPG Photonics [26]. An ARS Cryo cryostat was used to provide control of the temperature of the sample from 10.5 to 300 K. The cryostat used CaF_2 windows, which allowed transmission of mid-IR radiation. Fig. 3 shows the absorption spectrum of the sample from 14 K to 300 K.

Note that the absorption spectrum contains well-defined line-features which gradually broaden as the temperature of the sample increases. Fig. 4 shows the absorption spectrum taken at 10.5 K; the spectrum contains four sharp *zero-phonon lines* near 2700 cm^{-1} which correspond to transitions which are purely electronic, with no coupling to the lattice vibrations of the ZnSe host. We will show in the discussion which follows that much of the remaining structure is attributable to *phonon-assisted* transitions, which are broadened by phonon dispersion. These phonon-assisted transitions dominate the absorption spectra at $T > 30$ K.

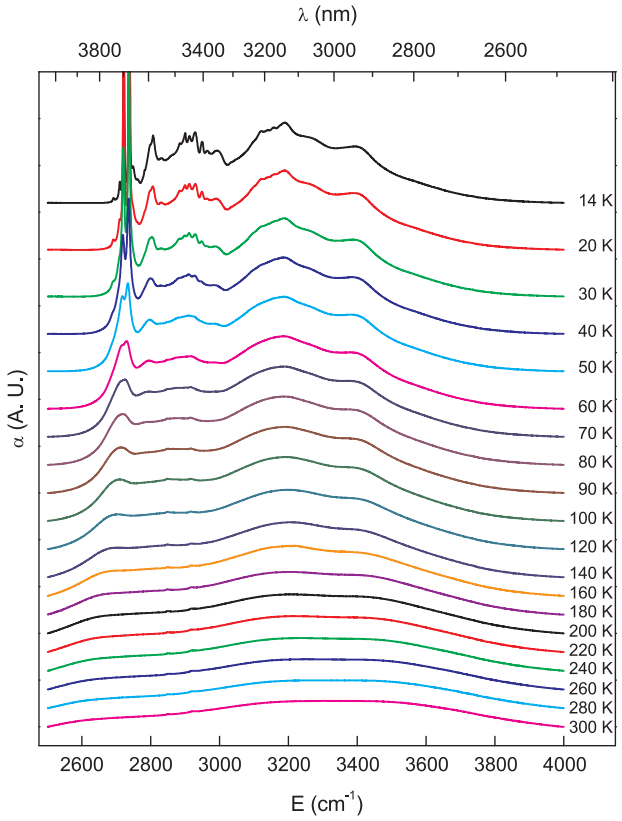

Fig. 3. The absorption spectra of Fe:ZnSe at a range of temperatures from 10.5 K to 300 K. The absorption spectrum at 10.5 K is shown in more detail in Fig. 4.

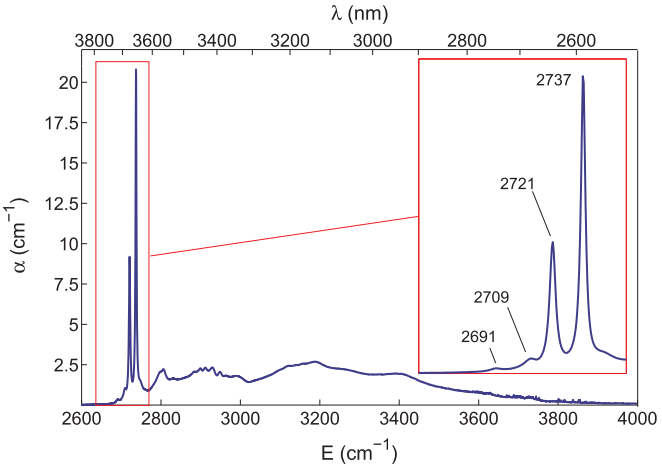

Fig. 4. The absorption spectrum of Fe:ZnSe at 10.5 K. The inset shows more detail of the four zero-phonon lines. The FTIR resolution was 1 cm^{-1}.

3.1. Discussion

From the measured spectra we determine values for Δ, λ, σ, Q, and W. We assume the following assignments for the transition energies corresponding to zero-phonon lines in the 10.5 K absorption spectrum:

$$E_{\Gamma_5} - E_{\gamma_1} = 2737 \text{ cm}^{-1} \quad (3a)$$

$$E_{\Gamma_5} - E_{\gamma_4} = 2721 \text{ cm}^{-1} \quad (3b)$$

$$E_{\Gamma_5} - E_{\gamma_3} = 2709 \text{ cm}^{-1} \quad (3c)$$

$$E_{\Gamma_5} - E_{\gamma_5} = 2691 \text{ cm}^{-1} \quad (3d)$$

$$E_{\Gamma_4'} - E_{\gamma_4} = 2929\ \mathrm{cm}^{-1} \tag{3e}$$

$$E_{\Gamma_5'} - E_{\gamma_1} = 2912\ \mathrm{cm}^{-1} \tag{3f}$$

The absorption coefficients corresponding to the allowed transitions are

$$\alpha_{nm} = \sigma_{nm} N_n = \frac{2}{3}\frac{\pi^2 \nu}{\epsilon_0 hc} g_{\Gamma_m} g_{\gamma_n} \mu_{nm}^2\, l(\nu - \nu_{nm}) \cdot \frac{g_{\gamma_n}}{g_{\gamma_1}} \exp\left(-\frac{E_{\gamma_n} - E_{\gamma_1}}{k_B T}\right)$$
$$\propto \left(E_{\Gamma_m} - E_{\gamma_n}\right) g_{\Gamma_m} g_{\gamma_n}^2 \mu_{nm}^2 \cdot \exp\left(-\frac{E_{\gamma_n} - E_{\gamma_1}}{k_B T}\right), \tag{4}$$

where σ_{nm} is the absorption cross-section, N_n is the fractional occupancy of the n^{th} lower level, g_{Γ_m} is the degeneracy of the m^{th} upper level, g_{γ_n} is the degeneracy of the n^{th} lower level, μ_{nm}^2 is the transition moment, $l(\nu - \nu_{nm})$ is the lineshape function, and the exponential term is the familiar Boltzmann expression which describes the thermal occupancy of the γ_n level relative to the γ_1 ground level. Note that, in the third line, we have used $g_{\gamma_1} = 1$.

If we suppose that DJT effects are not present in Fe:ZnSe, we can use the model of Udo [22] to describe the absorption spectrum. From Eqs. (3a) and (3b), we can generate four solution sets for Δ, λ, and $\sigma = |\lambda|/\Delta$. Only one of these solutions predicts lines which sensibly match the absorption spectrum of Fig. 4: $\Delta = 2949.3\ \mathrm{cm}^{-1}$, $\lambda = -99.72\ \mathrm{cm}^{-1}$ and $\sigma = 0.0338$. These parameters determine the energies of all nineteen $\gamma_n \rightarrow \Gamma_m$ transitions (see Eqs. (1) & (2)) and their relative absorption coefficients by Eq. 4. The degeneracy of each state is supplied by the model of Low and Weger [9] and the transition dipole moments by Udo et al. [22].

The model predicts three series of lines within the absorption spectrum of Fe:ZnSe as shown in Fig. 5a. The predictions of the model are seen to be only loosely consistent with the recorded absorption data. The transition energies of the zero-phonon lines are reasonably well matched, but their corresponding relative absorption coefficients exhibit poor agreement with the measured spectrum. Some additional lines are observed in the spectrum, but their energies and intensities are not well matched by the predictions of the model. Note the absence of the $\gamma_4 \rightarrow \Gamma_4'$ line, which is predicted to be dominant, from the collected spectrum.

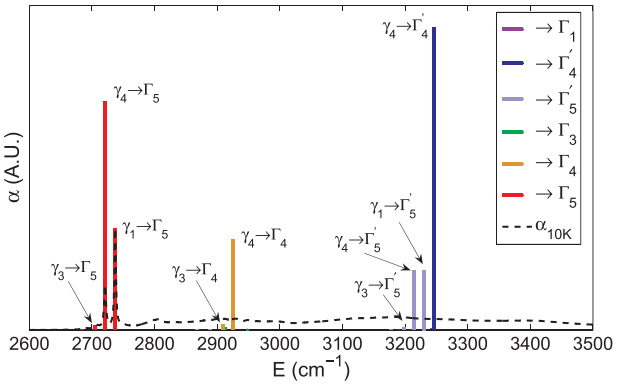

(a) Without the Dynamic Jahn–Teller effect

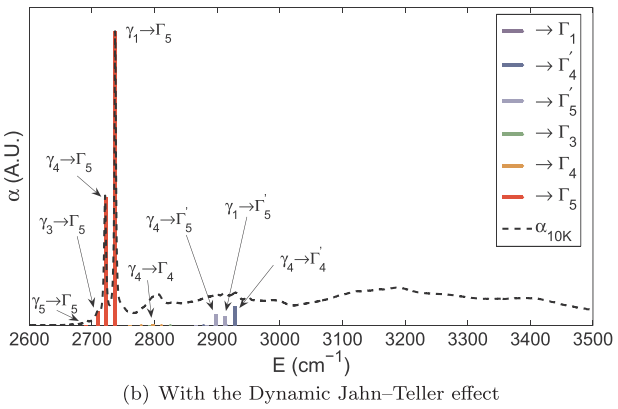

(b) With the Dynamic Jahn–Teller effect

Fig. 5. The fit of the allowed transitions of Fe^{2+} ions to the absorption spectrum of Fe:ZnSe at 10.5 K. (a) shows the purely electronic transitions when the DJT effect is not considered. (b) shows the purely electronic transitions when DJT effects are considered. The predicted line strengths were normalized to the 2737 cm^{-1} line of the collected absorption spectrum.

Table 2
The measured lifetime of several transitions of Fe:ZnSe. (a) Thermally resolved at 2691 cm^{-1}. (b) Spectrally resolved at 5 K.

T (K)	τ (μs)
5	49.4 ± 0.2
10	49.8 ± 0.6
20	51.7 ± 0.2
35	54.8 ± 0.2
50	59.2 ± 0.3
65	60.3 ± 0.3
80	65.1 ± 0.8
95	69.2 ± 0.3
110	67.7 ± 0.2
125	61.9 ± 0.4
135	54.1 ± 0.2
150	46.4 ± 0.4
155	43.8 ± 0.3
170	33.7 ± 0.07
185	22.3 ± 0.06
200	14.5 ± 0.03
215	8.52 ± 0.03
230	4.83 ± 0.01
245	2.66
260	1.56
275	0.96
290	0.65
305	0.58

E (cm^{-1})	τ (μs)
2735	48.1 ± 0.1
2722	48.9 ± 0.1
2709	48.9 ± 0.1
2693	48.4 ± 0.2
2674	48.5 ± 0.1
2656	48.2 ± 0.2
2616	49.4 ± 0.4
2585	49.3 ± 0.2
2525	48.7 ± 0.1
2511	48.9 ± 0.2
2455	48.5 ± 0.1

If we suppose that DJT effects are strongly present in Fe:ZnSe, we can use a modified version of the model of SHC [10] to describe the absorption spectrum. From Eqs. (3a) and (3c)–(3f), we can generate four solution sets for Δ, λ, σ, Q, and W. Again, only one of these predicts lines which sensibly match the absorption spectrum of Fig. 4: $\Delta = 2852.2\ \mathrm{cm}^{-1}$, $\lambda = -101.17\ \mathrm{cm}^{-1}$, $Q = 0.3784$, $W = 0.6617$, and $\sigma = 0.0359$.[2] Here we used the transition dipole moments modified from SHC as shown in Table 1 where we have used $x = -0.25$, $y = 1$, and $\beta = 0.052$.[3]

[2] We have used σ as a free parameter to allow the inclusion of a fifth feature from the absorption data. Note that the returned value is within 1% of the constrained value $\sigma = |\lambda|/\Delta = 0.0355$.

[3] SHC include x and y to describe a modification of the transition moments involving Γ_4 and Γ_5 levels by the DJT effect as shown in Table 1. They give exact expressions for x and y in the limit that $|\zeta|$ is on the order of $|\rho|$ (see Footnote 1), but we note that, for our parameterization, $|\zeta| \gg |\rho|$. Consequently, we have treated x and y as free parameters for simplicity and to adjust the relative intensities of the predicted features to match the absorption data.

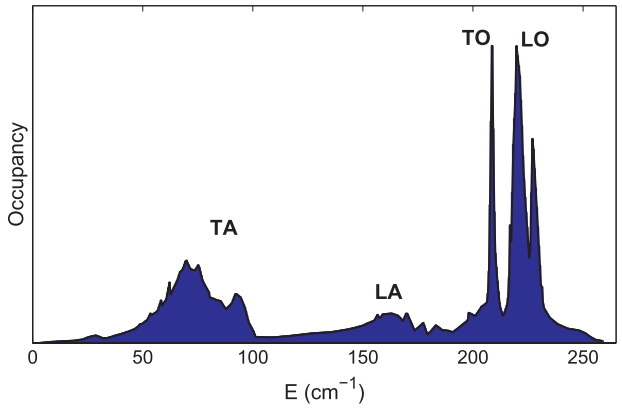

Fig. 6. The phonon density of states for room temperature ZnSe as determined by a linear combination of PDOS data from [12–14].

This model predicts one primary line-series of zero-phonon lines with two highly quenched series at slightly higher energies within the absorption spectrum as shown in Fig. 5b. The predictions of the model correspond very well to the recorded absorption spectrum. The transition energies of the zero-phonon lines are well matched and their corresponding absorption coefficients are in excellent agreement with the predicted values. The $\gamma_n \rightarrow \Gamma_{J' \neq 1}$ transitions are quenched such that they correspond well to the energy and magnitude of some observed lines from 2885 to 2930 cm^{-1}. This model is consistent with the 'alternative' assignment of the transition energies to the absorption spectrum of Fe:ZnS mentioned by SHC [10], which is characterized by a value of $|\lambda|$ which is a significant fraction of Δ and places the energies of transitions to $J' \neq 1$ levels at hundreds of cm^{-1} greater than the primary series.

Still, our determination of the transition energies and the corresponding relative absorption coefficients does not explain all the features in the observed absorption spectrum of Fe:ZnSe at 10.5 K. We attribute the structure at energies > 3000 cm^{-1} to transitions from the electronic levels in the ^5E manifold to vibronic energy levels in the $^5T_2$ manifold. To test this hypothesis, we extended our approximation of the absorption spectrum to include a vibrational component by convolution of the delta-like electronic transitions of Fig. 5b with the phonon density-of-states (PDOS) shown in Fig. 6. This curve was obtained by linear combination of the PDOS curves determined from inelastic neutron scattering (INS) data by Hennion [12] and Basak [13]. Multi-phonon contributions were roughly approximated by convolution with a 2×, 3×, and 4× energy scaling of the PDOS data.[4]

Fig. 7 shows the result of this convolution. This approximation to the absorption spectrum successfully explains much of the detail observed in the experimental absorption spectrum of Fe:ZnSe at 10.5 K. The TA-assisted feature at approximately 2800 cm^{-1} is clearly reproduced, structure in the 2885–2930 cm^{-1} region is reasonably approximated by electronic transitions acting in tandem with LO- and TO-assisted transitions, and structure at values >3000 cm^{-1} is approximated by multi-phonon assisted transitions.

Clearly, some of the structure is not accounted for, but the slight disparities are reasonably attributable to the difference between the idealized PDOS for room-temperature single-crystal ZnSe and the real PDOS in our sample of polycrystalline Fe:ZnSe at 10.5 K with disorder introduced by crystal defects, Fe^{2+} impurities, and nonuniform strain imparted by its polycrystalline nature. We attribute the difference between the measured spectrum and the calculated spectrum at energies >3000 cm^{-1} to two-mode mixing of phonons via the Jahn–Teller effect (see Fig. 5 of [24]). The agreement between the convolution and the measured absorption spectrum confirms that the basic picture we have developed of the distribution of states in the $^5T_2$ manifold is essentially correct.

The success of this calculation to approximate the observed absorption spectrum at 10.5 K suggests that transitions assisted by multiple phonons play a significant role in determining the absorption spectrum of Fe:ZnSe, especially at higher temperatures. In Fig. 3, the structure at energies >3000 cm^{-1} in the low-temperature absorption spectra is due to transitions involving the vibronic levels of the $^5T_2$ manifold and the structure at energies <2700 cm^{-1} is due to transitions involving the vibronic levels of the ^5E manifold. Such transitions become more probable with increasing temperature as the population of the vibronic levels of the ^5E manifold increases. The result is that the absorption spectrum broadens into a featureless continuum dominated by transitions which involve vibronic levels in both manifolds as shown in Fig. 3.

3.2. Section summary

In summary, we have seen that the absorption spectrum of Fe^{2+} ions in ZnSe changes drastically with sample temperature. We have shown that the model considered in the previous section qualitatively describes the optical behavior of Fe^{2+} ions in ZnSe. Furthermore, we observe that the transitions which do not terminate in the Γ_5 level are predicted by the spin–orbit model to be an order of magnitude stronger and at greater energies than observed, which suggests that spin-orbit quenching greatly reduces the dipole moment of such transitions, consistent with the DJT model of SHC [10] and the salient reduction of Van Vleck [25].

4. Fluorescence spectroscopy

A Cryo Industries of America (CIA) cryostat with CaF_2 windows was used to control the temperature of a $2 \times 6 \times 8$ mm^3 sample of Fe:ZnSe. The CVD-grown ZnSe sample was diffusion-doped with Fe^{2+} ions to a concentration of approximately 8.6×10^{18} cm^{-3} by IPG Photonics [26]. The cryostat was used in conjunction with a *Spectra-Pro 750* monochromator from Acton Research Co. to collect laser-induced fluorescence (LIF) spectra from 5 to 225 K as shown in Fig. 8. The sample was pumped using a Sheaumann *MIR-PAC* laser operating in the continuous-wave mode on the 2937 nm transition wavelength of Er:YAG. The chopped beam had approximately 200 mW of pump power at the sample.

Recall that, in the $^5T_2$ manifold, the Γ_4 level is separated from the Γ_5 level by >170 cm^{-1}. Also note that, at T = 5 K, $\exp(-E/k_bT)$ is essentially zero for $E > 20$ cm^{-1}. So, at thermal equilibrium, the population of the upper levels of the $^5T_2$ manifold will have essentially zero population and only transitions out of the Γ_5 level are expected in the emission spectrum.

Fig. 9 shows the LIF spectrum of the sample at 5 K. Note the approximate reciprocity of the emission spectrum with the absorption spectrum of Fig. 4 with strong emission on the same line series: 2691, 2709, 2721, and 2737 cm^{-1}. Thus, these emission lines are clearly attributable to $\Gamma_5 \rightarrow \gamma_n$ transitions.

Fig. 10 shows temperature-dependent LIF spectra of Fe:ZnSe recorded from 7.7 K to 220 K. Low-temperature data show clear phonon assisted transition lines near 2500 cm^{-1} which are absent at temperatures greater than 30 K. For temperatures greater than 100 K, the effect of thermally activated non-radiative quenching (NRQ) can be clearly seen as a decrease in the fluorescence per solid angle. Note that with every increase in the temperature of the sample, the peak of the Pekarian envelope is red-shifted slightly and the intensity can be seen to decrease for all wavelengths.

5. Lifetime measurements

Adams [1], Deloach et al. [16], and Jelínková et al. [17] have

[4] Mualin et al. [24] have shown that the Jahn–Teller coupling of the electronic Hamiltonian to acoustic modes of vibration is much stronger than to optical modes, so we have reduced the magnitude of the optical modes by factor of four in this convolution.

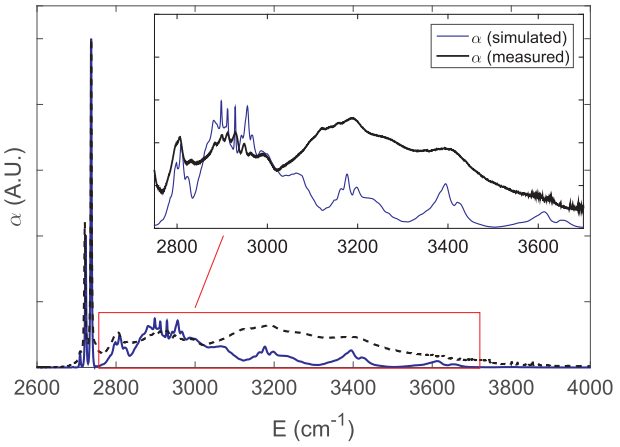

Fig. 7. The measured absorption spectrum (black) compared with the calculated absorption spectrum (blue) as determined by convolution[5] of the electronic transitions (Fig. 5b) of Fe:ZnSe with PDOS data (Fig. 6). The inset shows the highlighted region in additional detail.

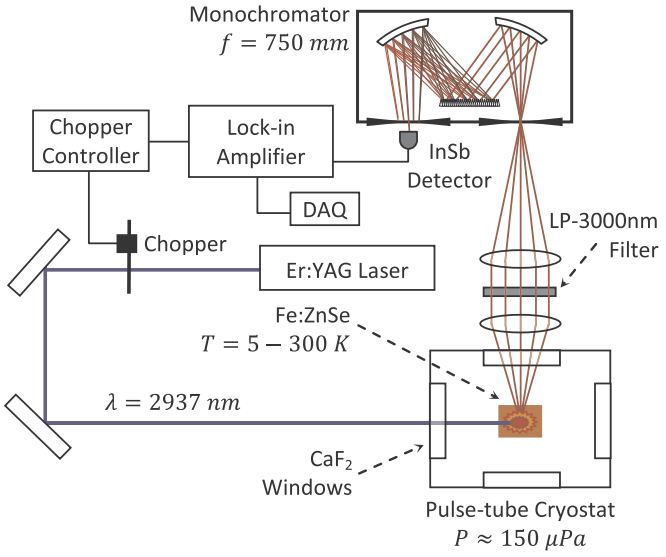

Fig. 8. The experimental setup used to collect the LIF spectrum of Fe:ZnSe.

reported the lifetime of melt-grown Fe:ZnSe to approach 105 μs near 120 K (see Fig. 11).[6] However, Myoung et al. have reported a maximum value of approximately 60 μs at 100 K for polycrystalline CVD-grown ZnSe diffusion doped with Fe^{2+} ions [27]. It is important to note that the density of Fe^{2+} ions in the Fe:ZnSe sample used by Adams was approximately two orders of magnitude greater than that used by Myoung.

Measurements of the fluorescence lifetime of Fe^{2+} ions in CVD-grown ZnSe were performed using a flashlamp-pumped Er:YAG laser with a spinning mirror Q-switch. The laser emitted at 2937 nm with an average pulse width of approximately 200–300 ns. Pulses from the Er:YAG laser were focused into same sample of Fe:ZnSe used in the LIF experiment. The decay of the optical output was recorded by focusing radiative emission through an Acton *Spectra-Pro 750* monochromator onto a liquid-nitrogen cooled InSb detector and the signal was recorded with an oscilloscope.

[5] In this convolution, we also included a Lorentzian lineshape function centered at 0cm^{-1} to impart finite spectral width to the electronic transitions.

[6] For the remainder of this article, we will treat Adams' data as representative of the melt-grown material, since it is more complete.

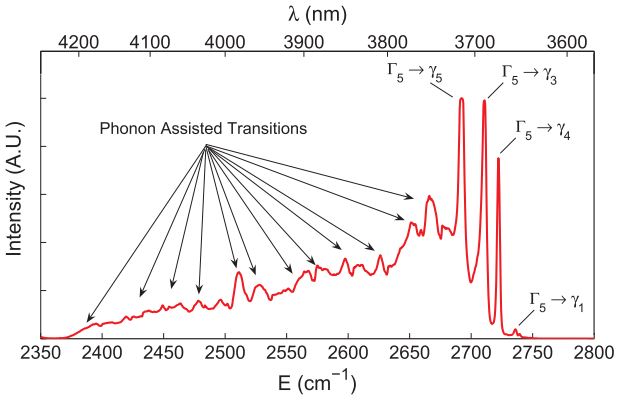

Fig. 9. The LIF of Fe:ZnSe at 5 K. The InSb detector was allowed to saturate to show the structure of weaker transitions. Thus, the intensity of the $\Gamma_5 \rightarrow \gamma_5$ feature is suppressed. The monochromator resolution was < 1 nm.

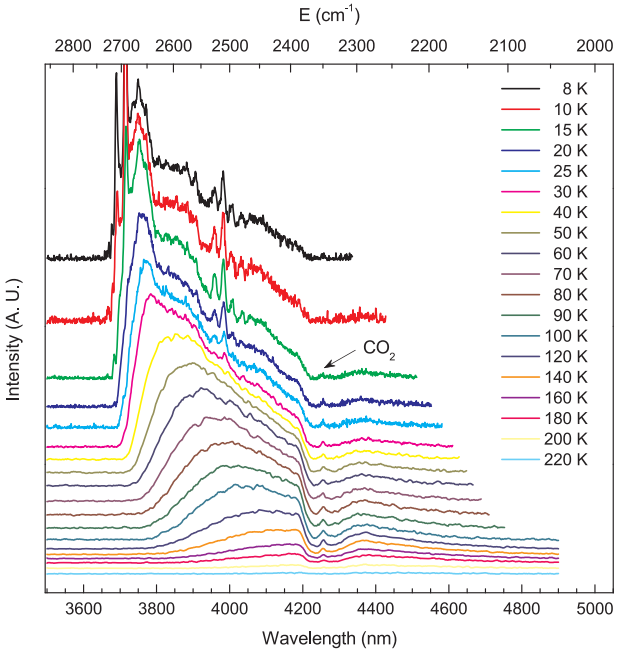

Fig. 10. Uncorrected temperature-dependent LIF spectra of Fe:ZnSe. The fluorescence efficiency is proportional to the integrated intensity of each curve, so we note that the radiative efficiency decreases with increasing temperature above 100 K. The valley near 2350 cm^{-1} is due to absorption by atmospheric CO_2.

The fluorescence lifetime τ of excited Fe^{2+} ions in ZnSe was determined as a least-squares fit of

$$I(t) = A\exp\left(-\frac{t - t_0}{\tau}\right) + a_0 \tag{5}$$

to the average pulse response of Fe:ZnSe. Datasets were collected from 5 K to 305 K in 15 K increments (see Table 2(a)). The temperature-dependent lifetime of Fe:ZnSe as measured by several authors is shown in Fig. 11.

The value of the fluorescence lifetime should be independent of wavelength if all the active ions in the sample are in thermal equilibrium. The decay trace of Fe:ZnSe at 5 K was recorded for the fluorescence peaks of Fig. 9. Table 2(b) shows the lifetime of Fe^{2+} in ZnSe as measured at these emission wavelengths. The data imply that the active population maintains thermal equilibrium throughout the decay process, implying that energy exchange between Fe^{2+} ions occurs at rates faster than the spontaneous decay.

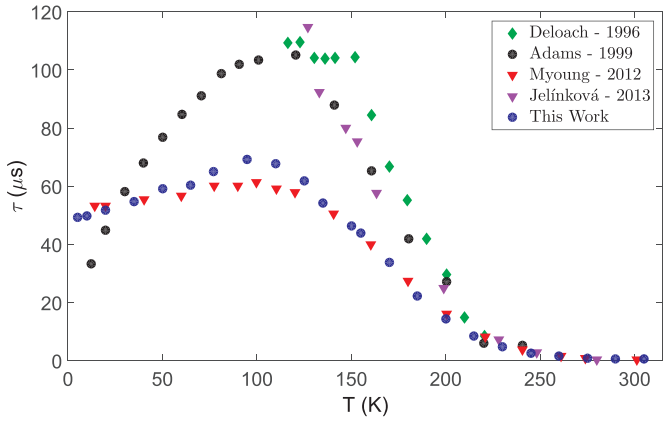

Fig. 11. The measured values of the fluorescence lifetime of Fe^{2+} ions in ZnSe with respect to changes in temperature.

5.1. Discussion

The Mott–Seitz model is the standard description of the temperature dependence of the fluorescence lifetime of optically active ions [28,29]. It describes the reduction of the fluorescence lifetime of these ions in terms of a purely radiative decay process competing with a thermally-activated non-radiative process. The observed fluorescence lifetime τ_{obs} of the ion depends on the relative probabilities that an excited ion will relax by each of these two processes. The total lifetime can be written

$$\tau_{total} = \tau_{rad}\cdot\eta = \tau_{rad}\cdot\frac{A_r}{A_r + A_{nr}\exp(-E/k_bT)}, \tag{6}$$

where τ_{rad} is the lifetime of the ion due to spontaneous radiative decay only, η is the fluorescence efficiency of the aggregate decay process, A_r is the probability of radiative decay, A_{nr} is the probability of non-radiative decay, and the exponential term is the familiar statistical term of Boltzmann with an activation energy E. This expression can be rewritten

$$\tau_{obs} = \frac{\tau_{rad}}{1 + C\exp(-E/k_bT)}, \tag{7}$$

and the parameters τ_{rad}, C, and E can be fit to match thermally-resolved lifetime data.

However, the Mott–Seitz model is not an adequate fit to the data collected for Fe:ZnSe, which exhibits an increasing trend with respect to temperature (at $T < 100$ K) that cannot be accommodated by this model. The non-radiative quenching term used in this model is also inadequate to describe trends in the temperature dependent lifetime of the Fe^{2+} ion in ZnSe. Consequently we have developed a new model which incorporates energy transfer and multi-phonon cascade statistics to describe the radiative and non-radiative decay processes respectively.

Eq. (7) can be recast in terms of related rates:

$$W_{obs} = W_{rad}(1 + C\exp(-E/k_bT)) \tag{8}$$

So written, it is clear that the Mott–Seitz model includes a radiative term and a non-radiative term.

In the Appendix, we derive an expression for W_{rad} which includes two terms which together describe the net effect of energy transfer mechanisms on the radiative lifetime of the upper manifold. In the first term, W_1 represents the combined rate of spontaneous decay and nonradiative energy transfer affecting lower energy levels in the $^5T_2$ manifold. In the second term, W_2 represents the combined rate of spontaneous decay and fluorescent re-absorption (with re-emission) affecting higher energy levels in the $^5T_2$ manifold. Energy exchange through the lattice allows the levels within the manifold to maintain thermal equilibrium. Thus, the observed decay is single-exponential and can be expressed as

Table 3
The returned values of the fit parameters for our model of the temperature-dependent fluorescence lifetime of Fe^{2+} ions in ZnSe. Note that A/M^2, p, and S are similar across columns.

N (cm^{-3})	Myoung [27] 1.0×10^{17}	This Work 8.6×10^{18}	Adams [1] $\sim5\times10^{19}$
A/M^2 (ns)	10.8 ± 0.7	10.2 ± 1.2	9.8 ± 2.4
τ_1 (μs)	54.5 ± 0.6	51.8 ± 1.0	34.5 ± 3.6
τ_2 (μs)	~80	~108	~245
ΔE (cm^{-1})	90.1 ± 15.9	94.0 ± 16.0	47.8 ± 5.9
S	5.46	5.47	5.44
p	16.0 ± 0.7	15.69 ± 0.3	17.2 ± 0.8
G_2/G_1	4.84 ± 0.25	5.64 ± 1.8	7.5 ± 0.9

$$W_{rad} = \frac{W_1}{1 + \frac{G_2}{G_1}\exp\left(-\frac{\Delta E}{k_bT}\right)} + \frac{W_2}{1 + \frac{G_1}{G_2}\exp\left(\frac{\Delta E}{k_bT}\right)}; \tag{9}$$

each of the parameters is defined in the Appendix.

We also replace the non-radiative term in Eq. 7 with the Miyakawa–Dexter expression for non-radiative quenching due to multi-phonon cascade [30] to obtain,

$$W_{obs} = W_{rad} + W_{nr}^{(p)}, \tag{10}$$

where

$$W_{nr}^{(p)} = \frac{A}{M^2\sqrt{2\pi p}}\left(\frac{Se}{p}\right)^{p-2}\left(1 + \frac{1}{\exp\left(\frac{h\nu_{eff}}{k_bT}\right) - 1}\right)^{p}, \tag{11}$$

and where k_b is Boltzmann's constant, e is Euler's constant, A is a coupling constant for the non-radiative term, M is an effective mass, and $h\nu_{eff} = E/p$ is the effective phonon energy required for p phonons to bridge the energy gap E between the energy levels involved in the optical transition.

Using this approach we can construct a model for the fluorescence lifetime $\tau_{total} = 1/W_{total}$ that includes both non-radiative quenching and thermal statistics:

$$W_{obs} = \frac{W_1}{1 + \frac{G_2}{G_1}\exp\left(-\frac{\Delta E}{k_bT}\right)} + \frac{W_2}{1 + \frac{G_1}{G_2}\exp\left(\frac{\Delta E}{k_bT}\right)} + \frac{A}{M^2\sqrt{2\pi p}}\left(\frac{Se}{p}\right)^{p-2}\cdot\left(1 + \frac{1}{\exp\left(\frac{h\nu_{eff}}{k_bT}\right) - 1}\right)^{p} \tag{12}$$

We eliminated ν_{eff} as a fit parameter by recasting it in terms of p and using the approximation that $E \approx \Delta = 2852\ cm^{-1}$. Thus, $h\nu_{eff} = \Delta/p$. Thus, we obtain a model that includes seven fit parameters: A/M^2, $\tau_1 = 1/W_1$, $\tau_2 = 1/W_2$, ΔE, S, p, and G_2/G_1. Table 3 shows the modeled values of these parameters as fit to the data of Adams et al. [1], Myoung et al. [27], and this work.

5.2. Analysis

The fit of the model represented in Table 3 to the lifetime data is excellent (see Fig. 12). The 90% confidence intervals are small and the increase of the radiative lifetime as T approaches 100 K is nicely accommodated. Thus, we conclude that our model accurately describes the increase observed in the fluorescence lifetime with increasing temperatures for $T < 100$ K. We attribute this increase to the fact that the upper levels in the $^5T_2$ manifold become more densely populated with increasing temperature, increasing the spectral overlap of absorp-

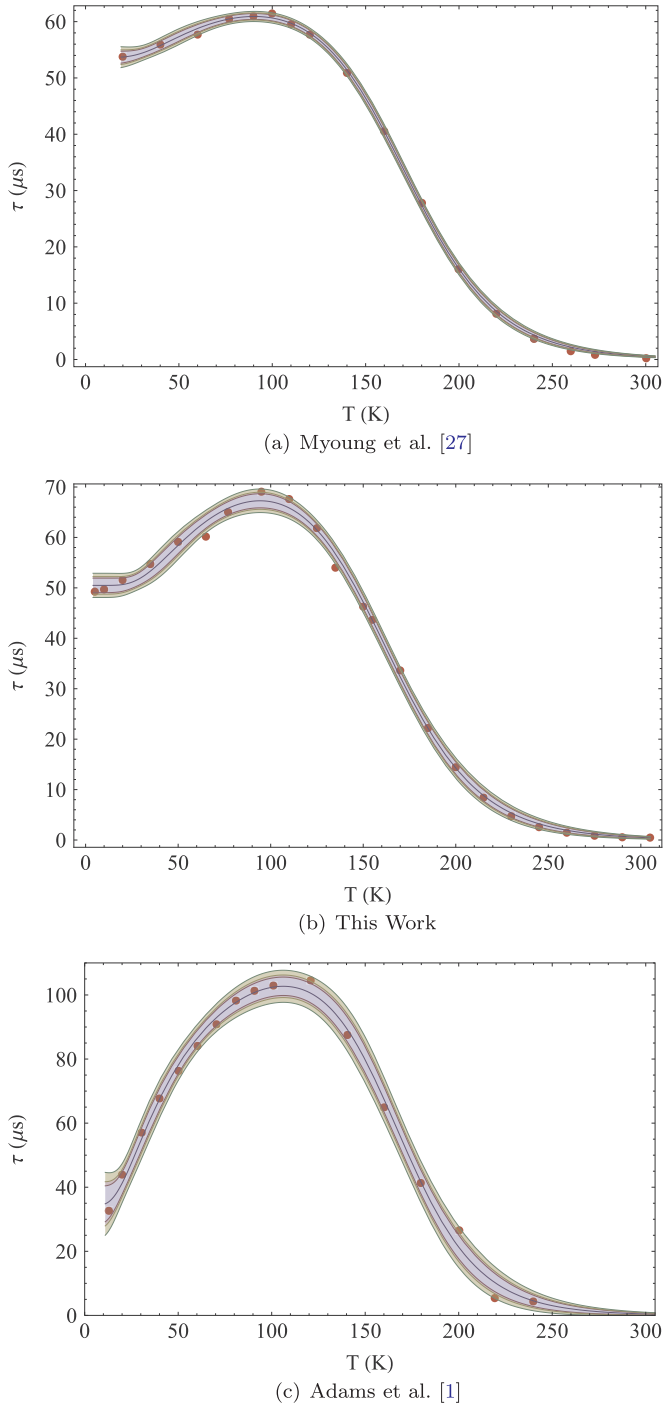

Fig. 12. A numerical fit of Eq. 12 to the lifetime data for diffusion-doped Fe:ZnSe. Colored bands show the 90%, 95%, and 99% confidence intervals.

tion and emission, and thereby increasing the rate of the absorption of fluorescence and subsequent re-emission. The decrease in lifetime for $T > 100$ K is confirmed to be due to NRQ. We also note that the effective phonon energy $h\nu_{eff} = E/p$ is approximately 160–175 cm^{-1}. This range is consistent with the phonon density distributions reported by Hennion [12], Rajput [14], and Basak [13] which we calculated to have centroids of approximately 162, 157, and 150 cm^{-1} respectively.

Note that the value of A^2/M, p, and S are virtually unchanged from sample to sample. However, the value of τ_1 decreases with increasing concentration, indicating that the rate of NRET increases with concentration. Similarly, the value of τ_2 increases with increasing dopant concentration, indicating that the rate of fluorescent re-absorption also increases with concentration. The relative degeneracy factor G_2/G_1 also increases with concentration and the value of ΔE is also sample-dependent, but the physical interpretation of these trends in not obvious. The primary difference between the datasets is the Fe^{2+} dopant concentration of the corresponding sample, so we conclude that the lifetime trend is determined primarily by the concentration of Fe^{2+} ions. From the data of Adams et al., we see that concentration effects dominate the spontaneous decay process at elevated Fe^{2+} concentrations.

5.3. Section summary

In summary, we have measured the fluorescence lifetime of Fe:ZnSe from 5 to 300 K. Our results are similar to the results of Myoung et al. [27]. Additionally, we have constructed a model which accurately describes previously ignored effects which determine the temperature dependence of the fluorescence lifetime of Fe:ZnSe. This model suggests that the Fe^{2+} concentration of the individual samples is responsible for the differences in total lifetime trends observed by Adams [1], Deloach et al. [16], and Jelínková et al. [17] ($\tau_{max} > 100$ μs) on one hand and by Myoung et al. [27] and in this work ($\tau_{max} < 70$ μs) on the other. The model also provides strong evidence that multi-phonon NRQ is responsible for the reduction of the fluorescence lifetime at temperatures >100 K.

6. Conclusions and future work

In conclusion, we have recorded absorption and emission spectra of CVD-grown ZnSe diffusion-doped with Fe^{2+} ions over a broad range of temperatures. We have directly observed sharp zero-phonon lines at 2691, 2709, 2721, and 2737 cm^{-1} in the low-temperature absorption and emission spectra and have assigned them to the $\gamma_5 \leftrightarrow \Gamma_5$, $\gamma_3 \leftrightarrow \Gamma_5$, $\gamma_4 \leftrightarrow \Gamma_5$, and $\gamma_1 \leftrightarrow \Gamma_5$ transitions respectively. We have augmented the parameterization of SHC and described the structure observed in the 10.5 K absorption spectrum in terms of allowed electronic transitions assisted by multiple phonons. Furthermore, we have shown that multi-phonon transitions play a significant role in determining the shape of the absorption spectrum of Fe:ZnSe.

We have measured the fluorescence lifetime of Fe:ZnSe with respect to temperature and confirmed that its temperature dependence is sensitive to the dopant concentration of the sample. Spectrally-resolved measurements of the lifetime were taken and were found to be consistent with an upper state manifold in thermal equilibrium during the decay process. We constructed a model which well explains thermal trends in the fluorescence lifetime. The model fits the drastically different datasets for Fe:ZnSe recorded by multiple authors. From this model, we confirm that thermally activated multi-phonon quenching is responsible for the reduction in the fluorescence efficiency of Fe:ZnSe and we show that the observed increase in lifetime with temperature in the 0–100 K range is a Fe^{2+} concentration effect.

Future efforts will proceed along two parallel fronts. First, the measurements and analyses of this work will be repeated across other crystal hosts for Fe^{2+} ions such as ZnS and CdMnTe. Second, we will further investigate the role of the Fe^{2+} dopant concentration in determining the observed fluorescence lifetime of Fe:ZnSe. An upcoming publication will present our study of concentration-activated energy transfer processes in Fe:ZnSe. The results of each study will be discussed in the context of engineering Fe:II–VI materials for use as gain media in mid-IR laser sources.

Acknowledgments

We acknowledge and thank the Sensors Directorate and the Air Force Office of Scientific Research (AFOSR) for funding this effort. We thank Doug Moore of Leidos Inc. for machining modifications to our cryostats and Ramesh Shori of SPAWAR for providing the pulsed

Er:YAG laser used to observe the fluorescence decay. Jonathan Evans thanks Glenn Perram, David Weeks, Nancy Giles, and Kevin Gross of the Air Force Institute of Technology (AFIT), Vladimir Fedorov of IPG Photonics, Sean McDaniel of Leidos, as well as Gary Cook, Rita Peterson, and Robert Bedford of the Sensors Directorate for technical discussions. B. Rami Reddy thanks AFOSR for providing a summer faculty fellowship. This research was performed while Thomas Harris held an NRC Research Associateship award at AFRL/RY.

Appendix A. Appendix: Derivation

Here, we will develop a description of the $^5T_2$ manifold in which the low-energy population experiences non-radiative energy transfer (NRET) between Fe^{2+} ions and the higher-energy population experiences significant re-absorption (with subsequent re-emission) of fluorescent radiation. NRET will shorten the observed lifetime from its intrinsic value and re-absorption will lengthen it.[7]

The average relaxation rate of the $^5T_2$ manifold is the simply the weighted sum of the relaxation rates of each of its sublevels

$$W_{rad} = \frac{1}{N}\sum_{n=1}^{M} N_n W_n, \tag{13}$$

where the total population is $N = \sum_n N_n$ and M is the total number of sublevels. For simplicity, we treat the manifold as consisting of two energy nondegenerate meta-levels. Level 1 has a population N_1 and undergoes NRET with some probability P_1. Level 2 has a population N_2 and undergoes re-absorption with some probability P_2 (we assume 100% re-emission).

It is useful to define a parameter that describes the partitioning of the manifold into these two meta-levels. The ratio of the degeneracies G_1 and G_2 of the meta-levels is

$$\frac{G_2}{G_1} = \frac{\sum_{n=m+1}^{M} g_n}{\sum_{n=1}^{m} g_n}, \tag{14}$$

where M is the total number of sublevels in the manifold and g_n is the degereneracy factor of the n^{th} level. However, this partitioning of the manifold is arbitrary, so G_2/G_1 can be treated as a fit parameter.[8]

We introduce thermal statistics by noting that the fractional population distribution is described by

$$\frac{N_2}{N_1} = \frac{G_2}{G_1}\exp\left(-\frac{\Delta E}{k_b T}\right), \tag{16}$$

where ΔE is the separation of the two meta-levels. Substituting Eq. 16 into Eq. 13, we find

$$W_{rad} = \frac{W_1}{1 + \frac{G_2}{G_1}\exp\left(-\frac{\Delta E}{k_b T}\right)} + \frac{W_2}{1 + \frac{G_1}{G_2}\exp\left(\frac{\Delta E}{k_b T}\right)}. \tag{17}$$

References

[1] J.J. Adams, C. Bibeau, R.H. Page, D.M. Krol, L.H. Furu, S.A. Payne, Lasing of Fe:ZnSe below 180 K, a new mid-infrared laser material, Opt. Lett. 24 (23) (1999) 1720–1722, http://dx.doi.org/10.1364/OL.24.001720.

[2] M.P. Frolov, Y.V. Korostelin, V.I. Kozlovsky, V.V. Mislavskii, Y.P. Podmar'kov, S.A. Savinova, Y.K. Skasyrsky, Study of a 2J pulsed Fe:ZnSe 4 μm laser, Laser Phys. Lett. 10 (12) (2013) 125001.

[3] A.A. Voronov, V.I. Kozlovskii, Y.V. Korostelin, A.I. Landman, Y.P. Podmar'kov, Y.K. Skasyrskii, M.P. Frolov, A continuous-wave Fe^{2+}:ZnSe laser, Quantum ElectronicsElectron. 38 (12) (2008) 1113.

[4] J.W. Evans, P.A. Berry, K.L. Schepler, 840 mW Continuous-wave Fe:ZnSe laser operating at 4140 nm, Opt. Lett. 37 (23) (2012) 5021–5023.

[5] J. Evans, P. Berry, K. Schepler, A passively Q-switched CW-pumped Fe:ZnSe laser, IEEE J. Quantum Electron. 50 (3) (2014) 204–2008, http://dx.doi.org/10.1109/JQE.2014.2302233 https://ieeexplore.iee.org/xpls/abs_all.jps?arnumber=6720174&tag=1.

[6] M. E. Doroshenko, H. Jelínková, T. T. Basiev, M. Jelínek, P. Koranda, M. Němec, V. K. Komar, A. S. Gerasimenko, V. V. Badikov, D. V. Badikov, D. Vyhlídal, J. Stoklasa, Fe:ZnSe laser - Comparison of Active Materials Grown by two Different Methods, Vol. 7912, 2011, pp. 79122D–79122D–6. ⟨http://dx.doi.org/10.1117/12.876082⟩ ⟨http://dx.doi.org/10.1117/12.876082⟩.

[7] J. J. Adams, C. Bibeau, R. H. Page, S. A. Payne, Tunable Laser Action at 4.0 microns from Fe:ZnSe, in: Advanced Solid State Lasers, Optical Society of America, 1999, p. WD3.⟨http://www.opticsinfobase.org/abstract.cfm?URI=ASSL-1999-WD3⟩.

[8] V.A. Akimov, A.A. Voronov, V.I. Kozlovskii, Y.V. Korostelin, A.I. Landman, Y.P. Podmar'kov, M.P. Frolov, Efficient lasing in a Fe^{2+}:ZnSe crystal at room temperature, Quantum Electron. 36 (4) (2006) 299 http://stacks.iop.org/1063-7818/36/i=4/a=A01.

[9] W. Low, M. Weger, Paramagnetic resonance and optical spectra of divalent iron in cubic fields. I. Theory, Phys. Rev. 118 (1960) 1119–1130, http://dx.doi.org/10.1103/PhysRev.118.1119 http://link.aps.org/doi/10.1103/PhysRev.118.1119.

[10] G.A. Slack, F.S. Ham, R.M. Chrenko, Optical absorption of tetrahedral fe^{2+} ($3d^6$) in cubic zns, cdte, and mg al_2o_4, Phys. Rev. 152 (1966) 376–402, http://dx.doi.org/10.1103/PhysRev.152.376 http://link.aps.org/doi/10.1103/PhysRev.152.376.

[11] F.S. Ham, G.A. Slack, Infrared absorption and luminescence spectra of Fe^{2+} in Cubic ZnS: role of the Jahn-Teller coupling, Phys. Rev. B 4 (1971) 777–798, http://dx.doi.org/10.1103/PhysRevB.4.777.

[12] B. Hennion, F. Moussa, G. Pepy, K. Kunc, Normal modes of vibrations in znse, Phys. Lett. A 36 (5) (1971) 376–378, http://dx.doi.org/10.1016/0375-9601(71)90267-2 http://www.sciencedirect.com/science/article/pii/0375960171902672.

[13] T. Basak, M.N. Rao, M. Gupta, S. Chaplot, Vibrational properties and phase transitions in ii-vi materials: lattice dynamics, ab initio studies and inelastic neutron scattering measurements, J. Phys.: Condens. Matter 24 (11) (2012) 115401.

[14] B. Rajput, D. Browne, Lattice dynamics of ii-vi materials using the adiabatic bond-charge model, Phys. Rev. B 53 (14) (1996) 9052.

[15] G.A. Slack, B.M. O'Meara, Infrared Luminescence of Fe^{2+} in ZnS, Phys. Rev. 163

[7] Henderson and Imbusch [19] provide a broad overview of the electronic dynamics of vibronic systems at high dopant concentrations. They note that phonon-assisted NRET between active ions occurs with greater probability with decreasing temperature and increasing dopant concentration. They also note that re-absorption of fluorescent radiation occurs with greater probability with increasing spectral overlap and with increasing ion concentration. The spectral overlap of the absorption and emission bands of Fe:ZnSe increases with increasing temperature due to the broadening of those bands as more levels become thermally accessible. The relative probabilities of these processes are mediated by the occupation statistics of the sublevels of the manifold, which have been seen to be in thermal equilibrium.

[8] If we ignore electron–phonon coupling in the $^5T_2$ manifold and construct the first meta-level from the three-fold degenerate Γ_5 level, and the second meta-level from the remaining twelve $^5T_2$ levels, the ratio becomes

$$\frac{G_2}{G_1} = \frac{12}{3} = 4. \tag{15}$$

So, we expect that the value of C will be on the order of 4 for any dataset.

(1967) 335–341, http://dx.doi.org/10.1103/PhysRev.163.335 http://link.aps.org/doi/10.1103/PhysRev.163.335.
[16] L. DeLoach, R. Page, G. Wilke, S. Payne, W. Krupke, Transition metal-doped zinc chalcogenides: spectroscopy and laser demonstration of a new class of gain media, IEEE J. Quantum Electron. 32 (6) (1996) 885–895, http://dx.doi.org/10.1109/3.502365.
[17] H. Jelínková, M.E. Doroshenko, M. Jelínek, D. Vyhlídal, J. Šulc, M. Němec, V. Kubeček, Y.A. Zagoruiko, N.O. Kovalenko, A.S. Gerasimenko, V.M. Puzikov, V.K. Komar, Fe:ZnSe Laser Oscillation Under Cryogenic and Room Temperature, Vol. 8599, 2013, pp. 85990E–85990E–7. ⟨http://dx.doi.org/10.1117/12.2003840⟩.
[18] Y. Tanabe, S. Sugano, On the absorption spectra of complex ions ii, J. Phys. Soc. Jpn. 9 (5) (1954) 766–779, http://dx.doi.org/10.1143/JPSJ.9.766 http://jpsj.ipap.jp/link?JPSJ/9/766/.
[19] B. Henderson, G.F. Imbusch, Optical Spectroscopy of Inorganic Solids, Monographs on the Physics And Chemistry of Materials, Clarendon Press, Oxford, 1989.
[20] H.A. Bethe, Splitting of terms in crystals, Ann. Phys. 3 (5) (1929) 133.
[21] J. Rivera-Iratchet, M.A. de Orúe, E.E. Vogel, Vibronic coupling and the near-infrared spectrum of Fe^{2+} in CdTe and ZnS, Phys. Rev. B 34 (1986) 3992–4001, http://dx.doi.org/10.1103/PhysRevB.34.3992 http://link.aps.org/doi/10.1103/PhysRevB.34.3992.
[22] M.K. Udo, M. Villeret, I. Miotkowski, A.J. Mayur, A.K. Ramdas, S. Rodriguez, Electronic excitations of substitutional transition-metal ions in II-VI semiconductors: CdTe:Fe^{2+} and CdSe:Fe^{2+}, Phys. Rev. B 46 (1992) 7459–7468, http://dx.doi.org/10.1103/PhysRevB.46.7459 http://link.aps.org/doi/10.1103/PhysRevB.46.7459.
[23] D. Colignon, E. Kartheuser, S. Rodriguez, M. Villeret, Excitation Spectrum of Fe^{2+} in a tetrahedral potential: dynamic Jahn-Teller Effect, Phys. Rev. B 51 (8) (1995) 4849.
[24] O. Mualin, E.E. Vogel, M.A. de Orúe, L. Martinelli, G. Bevilacqua, H.-J. Schulz, Two-mode Jahn-Teller effect in the absorption spectra of Fe^{2+} in II-VI and III-V semiconductors, Phys. Rev. B 65 (2001) 035211, http://dx.doi.org/10.1103/PhysRevB.65.035211 http://link.aps.org/doi/10.1103/PhysRevB.65.035211.
[25] J. van Vleck, Note on the gyromagnetic ratio of Co^{++} and on the Jahn-Teller effect in Fe^{++}, Physica 26 (7) (1960) 544–552.
[26] IPG Photonics, personal communication.
[27] N. Myoung, V.V. Fedorov, S.B. Mirov, L.E. Wenger, Temperature and concentration quenching of Mid-IR photoluminescence in iron doped ZnSe and ZnS laser crystals, J. Lumin. 132 (3) (2012) 600–606, http://dx.doi.org/10.1016/j.jlumin.2011.10.00 http://www.sciencedirect.com/science/article/pii/S0022231311005758.
[28] V. Pagonis, C. Ankjaergaard, A. Murray, M. Jain, R. Chen, J. Lawless, S. Greilich, Modelling the thermal quenching mechanism in quartz based on time-resolved optically stimulated luminescence, J. Lumin. 130 (5) (2010) 902–909 http://dx.doi.org/10.1016/j.jlumin.2009.12.032 ⟨http://www.sciencedirect.com/science/article/pii/S0022231309006346⟩.
[29] N. F. Mott, R. W. Gurney, Electronic Processes in Ionic Crystals, Dover New York, 1964.
[30] T. Miyakawa, D.L. Dexter, Phonon sidebands, multiphonon relaxation of excited states, and phonon-assisted energy transfer between ions in solids, Phys. Rev. B 1 (1970) 2961–2969, http://dx.doi.org/10.1103/PhysRevB.1.2961 http://link.aps.org/doi/10.1103/PhysRevB.1.2961.